Heat Capacity of the Halogen-Bridged Mixed-Valence Complex Pt 2 (dta) 4 I (dta = CH 3 CS 2 -) †

ARTICLE *in* THE JOURNAL OF PHYSICAL CHEMISTRY B · JANUARY 2002

Impact Factor: 3.3 · DOI: 10.1021/jp013038m

8 AUTHORS, INCLUDING:

Michio Sorai
Osaka University
239 PUBLICATIONS **4,086** CITATIONS

Heat Capacity of the Halogen-Bridged Mixed-Valence Complex $Pt_2(dta)_4I$ (dta = $CH_3CS_2^-$)†

Yuji Miyazaki,‡ Qi Wang,§ Akane Sato,‡ Kazuya Saito,‡ Masahiro Yamamoto,⊥ Hiroshi Kitagawa,|| Tadaoki Mitani,⊥ and Michio Sorai*,‡

Research Center for Molecular Thermodynamics, Graduate School of Science, Osaka University, Toyonaka, Osaka 560-0043, Japan, Department of Chemistry, Zhejiang University, Hangzhou 310027, P. R. China, Department of Physical Materials Science, School of Materials Science, Japan Advanced Institute of Science and Technology, Tatsunokuchi, Ishikawa 923-1292, Japan, and Department of Chemistry, University of Tsukuba, 1-1-1 Tennodai, Tsukuba, Ibaraki 305-8571, Japan.

Received: August 7, 2001; In Final Form: October 15, 2001

Heat capacity of the halogen-bridged mixed-valence complex $Pt_2(dta)_4I$ (dta = $CH_3CS_2^-$) has been measured in the temperature region between 6 and 386 K. The complex exhibited a phase transition of order−disorder type at T_{trs} = 373.4 K, from being arranged in an ordered helical form of four dta ligand planes around the central Pt−Pt axis to dynamically jumping between two orientations. Neither latent heat nor distinct thermal hysteresis was observed for the phase transition, suggesting that the phase transition is of higher-order rather than of first-order. The transition enthalpy and entropy were determined to be $\Delta_{trs}H = 1.91 \pm 0.02$ kJ mol^{-1} and $\Delta_{trs}S = 5.25 \pm 0.07$ J K^{-1} mol^{-1}, respectively. The transition entropy close to R ln 2 (= 5.76 J K^{-1} mol^{-1}), where R is the gas constant, implies that the twisting motion of the four dta ligands takes place in a synchronized way. No thermal anomaly was detected around 300 and 90 K, where a Mott transition from the one-dimensional metallic phase to the semiconducting phase and a spin-Peierls-like transition have been expected. The reason for the absence of these transitions in calorimetry is discussed briefly.

1. Introduction

One-dimensional substances have drawn great attention in the field of chemistry and physics in that they exhibit specific electrical, magnetic, and optical properties.[1] Particularly, halogen-bridged one-dimensional mononuclear-metal complexes, the so-called MX-chain complexes, are suitable substances to research one-dimensional electron−electron or electron−lattice interaction.[2−4] The MX-chain compounds with M = Ni, Pd, and Pt and X = Cl, Br, and I are classified into two types of electronic state: Mott−Hubbard state[5−7] and charge-density-wave (CDW) state.[8−10] Up to now, however, no metallic behavior has been found in these systems.

Recently, a new one-dimensional system called MMX-chain complexes has drawn a great attention. MMX-chain complexes have more possible electronic states than MX-chain complexes:

$$\cdots X^-—M^{2.5+}\text{-}M^{2.5+}—X^-—M^{2.5+}\text{-}M^{2.5+}—X^-—M^{2.5+}\text{-}M^{2.5+}—X^-\cdots \quad \text{(I)}$$

$$\cdots X^-—M^{2+}\text{-}M^{2+}—X^-\text{-}M^{3+}\text{-}M^{3+}\text{-}X^-—M^{2+}\text{-}M^{2+}—X^-\text{-}M^{3+}\text{-}M^{3+}\text{-}X^-\cdots \quad \text{(II)}$$

$$\cdots X^-—M^{2+}\text{-}M^{3+}\text{-}X^-—M^{2+}\text{-}M^{3+}\text{-}X^-—M^{2+}\text{-}M^{3+}\text{-}X^-—M^{2+}\text{-}M^{3+}\text{-}X^-\cdots \quad \text{(III)}$$

$$\cdots X^-—M^{2+}\text{-}M^{3+}\text{-}X^-\text{-}M^{3+}\text{-}M^{2+}—X^-—M^{2+}\text{-}M^{3+}\text{-}X^-\text{-}M^{3+}\text{-}M^{2+}—X^-\cdots \quad \text{(IV)}$$

Mode I is an averaged-valence (AV) state, in which two possibilities are expected: a Mott−Hubbard insulator ($U > W \approx 4t$, where U, W, and t are the on-site Coulomb repulsion, bandwidth, and transfer integral, respectively) and a one-dimensional metal ($U < W$). Mode II is a mixed-valence insulating (CDW) state, where doubling of the unit cell occurs. Modes III and IV are charge-polarization (CP) and alternate-charge-polarization (ACP) states, respectively, where there exists an unpaired electron and thus spin at a Pt^{3+} site per dimer unit. In the case of mode III, as no cell doubling occurs, either a Mott−Hubbard insulator or a one-dimensional metal is expected. On the other hand, mode IV is expected to be an insulator analogous to a spin-Peierls state.

Two main families of the MMX-chain compounds have so far been reported: $A_4[Pt_2(pop)_4X_4]\cdot nH_2O$ (A = Li, K, Cs, NH_4; pop = diphosphonate, $H_2P_2O_5^{2-}$; X = Cl, Br, I)[11−18] and $M_2(dta)_4I$ (M = Ni, Pt; dta = dithioacetate, $CH_3CS_2^-$).[19−33] Interestingly, electrical conductivity and thermoelectric power measurements for a single crystal of $Pt_2(dta)_4I$ parallel to the chain axis b[24,25,28,29] revealed that this complex indicates a metallic temperature dependence above a metal−semiconductor transition temperature T_{M-S} = 300 K. Polarized reflectance spectra of a single crystal at room temperature[24,28] also indicated that a Drude-like reflectance associated with interbinuclear charge transfer was observed for the polarization parallel to the chain axis ($E||b$), which suggests that $Pt_2(dta)_4I$ is a one-dimensional metal. A metallic behavior was first observed in

† Contribution No. 51 from the Research Center for Molecular Thermodynamics.

* Corresponding author. Tel: +81-6-6850-5523. Fax: +81-6-6850-5526. E-mail: sorai@chem.sci.osaka-u.ac.jp.

‡ Osaka University.

§ Zhejiang University.

⊥ Japan Advanced Institute of Science and Technology.

|| University of Tsukuba.

10.1021/jp013038m CCC: $22.00
Published on Web 12/12/2001

TABLE 1: Molar Heat Capacities of $Pt_2(dta)_4I$ Crystal (M = 881.78 g mol^{-1})

T (K)	C_p (J K^{-1} mol^{-1})	T (K)	C_p (J K^{-1} mol^{-1})	T (K)	C_p (J K^{-1} mol^{-1})	T (K)	C_p (J K^{-1} mol^{-1})	T (K)	C_p (J K^{-1} mol^{-1})	T (K)	C_p (J K^{-1} mol^{-1})
Series 1		91.29	211.5	251.21	384.8	321.56	436.6	233.79	370.1	326.51	443.6
6.34	3.816	93.28	214.9	254.25	386.0	323.62	438.6	236.79	373.1	329.51	446.3
6.53	4.205	95.28	218.3	257.29	388.6	325.68	441.8	239.79	375.7	332.52	448.9
6.78	4.568	97.27	221.6	260.33	391.5	327.74	443.9	242.78	378.1	335.52	451.2
7.09	5.164	99.27	224.8	263.37	393.7	331.85	449.0	245.78	380.3	338.53	452.9
7.45	5.783	101.27	228.1	266.40	395.8	333.92	450.7	248.78	382.4	341.53	454.7
7.84	6.778	103.27	231.2	269.44	398.0	338.03	454.0	251.78	384.4	344.53	457.5
8.31	7.912	105.28	234.2	272.48	400.3	342.15	456.9	254.78	386.6	347.53	461.0
8.78	8.900	107.28	237.4	275.52	402.6	344.21	458.9	257.78	389.5	350.53	465.4
9.28	9.977	109.29	240.3	278.56	405.1	346.26	461.0	260.77	392.6	353.52	470.3
9.78	11.40	111.30	243.4	281.60	408.0	348.31	463.5	263.77	394.8	356.51	476.8
10.34	12.54	113.31	246.4	284.64	410.4	350.35	467.3	266.77	396.4	359.50	485.1
10.99	13.99	115.32	249.1	287.67	412.4	352.40	470.1	269.77	398.1	362.48	497.3
11.68	15.80	117.32	251.9	290.71	415.5	354.44	475.6	272.77	400.4	365.45	513.4
12.42	17.63	119.34	254.9	293.74	416.8	356.47	478.8	275.77	403.4		
13.21	19.61	121.35	257.8	296.77	419.5	358.51	483.6	278.77	406.1	Series 6	
14.03	21.78	123.36	260.3	299.80	422.0	360.53	490.5	281.77	407.4	297.98	420.7
14.87	24.10	125.37	263.3	302.84	423.8	362.56	499.4	284.77	409.7	300.99	422.0
15.73	26.43	127.38	266.3	305.88	426.7	364.59	509.8	287.77	411.4	303.99	425.1
16.65	28.74	129.40	268.8	308.91	428.4	366.61	521.3	290.77	414.5	307.00	427.5
17.64	32.08	131.41	271.1	311.95	431.5	368.63	535.2	293.78	416.4	310.01	428.7
18.62	34.87	133.43	273.6	314.98	434.4	370.64	556.6	296.78	417.8	313.02	433.6
19.63	37.92	135.44	276.3	318.02	437.9	372.64	593.6	299.78	420.0	316.03	435.6
20.67	41.21	137.46	278.6	321.05	440.9	374.66	566.8	302.79	423.0	319.04	439.4
21.74	44.07	139.48	280.7	324.09	444.5	376.73	524.3	305.80	425.0	322.05	439.4
22.84	47.91	141.50	283.2	327.13	447.7	378.79	506.9	308.81	426.4	325.07	441.7
23.94	51.60	143.52	285.5	330.18	451.1	380.83	498.2	311.82	433.6	328.09	445.5
25.09	54.85	145.53	288.3	333.22	454.4	382.87	493.7	314.83	434.9	331.11	447.5
26.35	58.79	147.55	291.4	336.28	458.4	384.90	490.4	317.86	435.6	334.14	450.0
27.70	63.00	149.57	293.3	339.34	460.6			320.88	436.4	337.17	452.6
29.05	67.28	151.59	295.3	342.38	462.0	Series 3		323.90	439.5	340.20	454.0
30.41	71.47	153.61	297.5	345.42	465.0	257.53	389.9	326.92	442.1	343.22	457.0
31.78	75.12	155.63	300.0	348.46	469.0	260.52	391.9	329.95	444.9	346.25	459.7
33.15	79.21	157.65	302.0	351.50	473.3	263.53	394.3	332.97	447.1	349.27	463.1
34.53	83.74	159.67	303.7	354.53	477.6	266.53	396.6	335.98	449.6	352.29	467.6
35.91	87.88	161.69	306.1	357.57	484.1	269.54	398.7	339.00	451.9	355.30	473.8
37.30	91.57	163.71	308.4	360.59	494.1	272.54	400.6	342.02	455.0	358.30	481.7
38.70	95.84	165.74	310.6	363.62	508.7	275.54	403.1	345.03	458.3	361.30	492.2
40.11	100.1	167.76	312.6	366.62	524.0	278.55	405.5	348.04	461.3	364.27	507.7
41.52	103.7	169.78	314.5	369.61	547.0	281.55	407.3	351.04	465.1	367.23	525.1
42.93	107.8	171.80	316.5	372.55	591.1	284.55	409.3	353.54	470.1	370.16	550.4
44.35	111.4	173.82	318.3	375.51	548.4	287.55	412.4	355.53	475.4	373.04	592.3
45.77	115.3	175.84	320.6	378.53	510.8	290.55	415.5	357.53	480.2	375.94	537.6
47.20	117.9	177.87	322.3	381.60	497.5	293.56	416.9	359.52	486.9	378.90	505.7
48.63	121.9	179.89	324.5	384.69	491.8	296.56	417.8	361.50	494.4	381.90	495.2
50.07	125.9	181.91	326.4			299.56	421.0	363.49	504.3	384.91	490.6
51.53	128.8	183.93	328.3	Series 2		302.57	423.1	365.47	515.5		
52.99	133.0	185.96	330.1	272.59	401.2	305.57	424.2	367.46	526.9	Series 7	
54.45	137.1	187.98	331.6	274.61	402.6	308.58	429.1	369.43	542.6	354.36	475.4
55.91	140.5	190.00	333.7	276.65	404.1	311.58	430.7	371.41	569.1	357.35	483.2
57.38	144.0	192.03	335.7	278.68	405.9	314.59	433.7	373.36	597.5	360.32	492.7
58.85	146.5	194.05	337.5	280.71	407.2	317.60	435.5	375.34	549.0	363.28	504.1
60.32	150.7	196.07	339.2	282.75	408.6	320.61	436.7	377.37	517.3	366.22	519.7
61.79	153.9	198.09	341.0	284.78	410.7	323.63	438.8	379.44	502.7	369.14	540.5
63.26	157.0	200.12	342.8	286.81	413.1	326.64	442.8	381.53	495.2	372.01	581.4
64.74	158.9	202.64	344.9	288.85	413.5	329.66	445.6	383.64	491.9	374.88	562.0
66.22	163.1	205.68	347.7	290.89	415.4	332.68	448.3	385.76	489.1	377.80	512.5
67.70	166.3	208.71	350.4	292.92	415.7	335.69	450.5			380.77	497.2
69.18	170.0	211.74	352.8	294.96	416.8	338.71	452.7	Series 5		383.77	490.6
70.66	173.0	214.77	355.3	297.00	418.1	341.72	455.5	290.49	415.4		
72.15	175.8	217.81	357.5	299.04	420.6	344.74	457.6	293.49	417.2		
73.64	179.2	220.84	360.0	301.09	421.1	347.75	460.3	296.49	418.6		
75.13	180.7	223.88	362.6	303.13	421.6	350.75	465.7	299.49	421.3		
76.62	184.9	226.91	364.8	305.17	424.2			302.50	423.5		
78.11	186.8	229.95	367.4	307.22	425.9	Series 4		305.50	425.7		
79.60	190.4	232.98	369.8	309.26	426.1	215.79	355.3	308.50	427.3		
81.34	193.5	236.02	371.6	311.31	427.8	218.79	358.1	311.50	432.4		
83.32	197.5	239.05	374.1	313.36	429.4	221.79	360.6	314.49	435.3		
85.31	201.4	242.09	376.9	315.40	431.5	224.79	363.1	317.50	437.4		
87.30	204.6	245.13	379.9	317.45	433.7	227.79	365.7	320.50	438.0		
89.29	208.1	248.17	382.6	319.51	435.1	230.79	368.1	323.51	440.5		

$Pt_2(dta)_4I$ among halogen-bridged one-dimensional transition-metal complexes. This metal−semiconductor transition was also confirmed by magnetic susceptibility measurement for a polycrystalline sample.[28,29]

Furthermore the temperature dependence of the electrical conductivity and thermoelectric power measurements[24,25,28,29] showed a first-order phase transition around 360 K. From single-crystal X-ray structure analyses,[24,25,32] it was revealed that a first-order phase transition occurs at $T_{trs} = 365$ K from the low-temperature phase with space group $C2/c$ to the high-temperature phase with $A2/m$ in which the cell volume is a half of that of the low-temperature phase. Also revealed is that this phase transition is of order−disorder type from being arranged in an ordered helical form of four dta ligand planes tilted around the central Pt−Pt axis by ca. 20 ° to dynamically jumping between two orientations. Differential scanning calorimetry (DSC)[32] also found an endothermic peak around 360 K on heating and a hysteresis characteristic of a first-order phase transition. In the initial experiments of the electrical conductivity measurements and single-crystal X-ray structure analyses,[24,25] an unusual negative hysteresis was observed, in which the low-temperature phase was transformed at 300 K on heating but the reverse transition occurred at 350 K on cooling. However, in the succeeding experiments,[28,29] such an anomalous negative hysteresis was not detected.

In the semiconducting phase below T_{M-S}, a knee-shaped anomaly was observed around 230 K in the electrical conductivity measurement,[28,29] which is related to an anomalous negative temperature dependence of the lattice constant a.[31−33] Moreover the magnetic susceptibility exhibited a convexity at 90 K, which seems to be a phase transition.[28,29]

From variable-temperature infrared (IR) spectroscopy,[26,28−30] polarized Raman spectroscopy at room temperature,[26,28−30] and ^{129}I Mössbauer spectroscopy at 16 and 80 K[27−29] together with the experimental results mentioned above, it is expected that the $Pt_2(dta)_4I$ complex is in a one-dimensional metallic phase with mode (I) above $T_{M-S} = 300$ K, in a semiconducting phase with mode (III) between 90 and 300 K, and in an insulating phase with mode (IV) below 90 K, despite the situation of the bridging I^- ions at the midpoints of two $Pt_2(dta)_4$ dimers.[19,24,25,31−33] Very recent low-temperature X-ray single-crystal analysis[31] suggested that a slight increase of the β value below 90 K might relate to the expected spin-Peierls distortion associated with dta ligand twisting. Quantum chemical calculations[34,35] suggested that Peierls distortion in the $Pt_2(dta)_4I$ chain can be played by the twisting distortion of dta ligand, resulting in mode (IV) of distribution of valence state. Yamamoto[36,37] showed by theoretical study that $Pt_2(dta)_4I$ should be regarded as a *d*-*p*-hybridized two-band material.

In this work, we investigate thermal properties of the $Pt_2(dta)_4I$ complex by adiabatic heat capacity measurement. Adiabatic calorimetry enables us to obtain precise and accurate heat capacities of substances, which is very useful to detect the existence of phase transitions, the exact thermodynamic quantities arising from phase transitions, and so on. In the present paper, we report the nature of the phase transition at $T_{trs} = 373.4$ K observed in the $Pt_2(dta)_4I$ crystal. We also carefully examined whether the other 'transitions' associated with the electronic structure change at 90 and 300 K manifest themselves in adiabatic heat capacity measurement.

2. Experimental Section

Crystals of $Pt_2(dta)_4I$ were synthesized according to the method described elsewhere.[26] We employed a low-temperature adiabatic calorimeter for small samples[38] to measure heat capacities of the sample from 6 to 386 K. The sample (1.67667 g) was loaded in a gold-plated copper cell and sealed together with helium gas at ambient pressure by an indium gasket. The helium gas works as a heat exchange medium. Buoyancy correction was made to obtain the true sample mass by use of the density of the crystal 3.133 g cm^{-3}.[26]

As for ac calorimetry, a single crystal with a typical dimension of 0.5 × 0.11 × 0.04 mm^3 was glued on a crossing point of Chromel versus Constantan thermocouples (13 μm in diameter) by use of gold paste. The sample was heated periodically at 2 Hz by chopped white light from a stabilized halogen lamp. The details of the ac calorimeter is described elsewhere.[39]

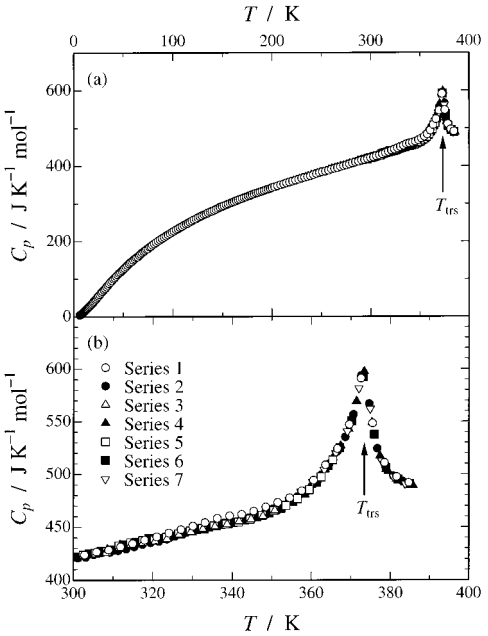

Figure 1. Molar heat capacities of $Pt_2(dta)_4I$ crystal (a) in the whole temperature region and (b) in the vicinity of the phase transition.

TABLE 2: Optimized Parameters of the Normal Heat Capacity Functions

	parameter	degeneracy
lattice vibration	$\Theta_D/K = 47.2 \pm 0.6$	$3N_A$
molecular libration	$\Theta_E/K = 66.8 \pm 1.1$	$3N_A$
intramolecular vibration	$\Theta_E/K = 124.1 \pm 0.4$	$11N_A$
	$\Theta_E/K = 341.7 \pm 1.5$	$5N_A$
	$\Theta_E/K = 798 \pm 19$	$6N_A$
	$\Theta_E/K = 2350 \pm 330$	$11N_A$
$(C_p - C_v)$ correction	$A \times 10^7/J^{-1}$ mol $= 2.05 \pm 0.41$	

3. Results and Discussion

Molar heat capacities of the $Pt_2(dta)_4I$ crystal are listed in Table 1 and plotted in Figure 1. In series 1, the virginal crystal was cooled from room temperature down to 6 K and then measurement was started. A distinct heat capacity peak due to a phase transition was observed at $T_{trs} = 373.4$ K. The transition temperature agrees well with the value obtained from the other experiments.[24,25,28,29,32] In the vicinity of the transition temperature, no latent heat characteristic of a first-order phase transition was observed. To see reproducibility of this phase transition and to check closely the thermal behavior around 300 K, heat capacity measurements were repeated in series 2, 4, and 6, and in series 2 to 5, respectively. The heat capacities in series 1 were greater than those in the other series in the range between 320 and 360 K, where an exothermic effect was observed. The

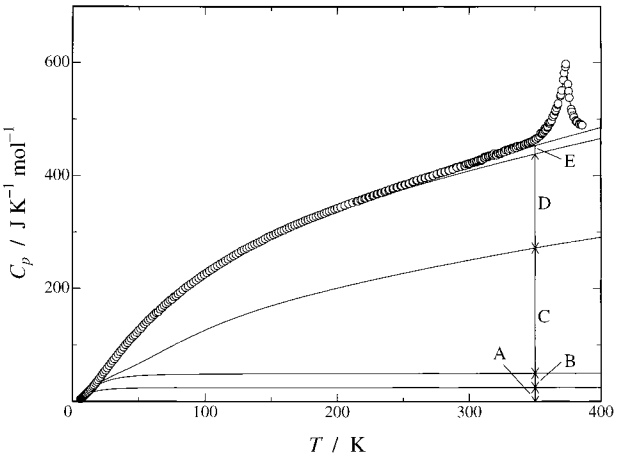

Figure 2. Molar heat capacities of $Pt_2(dta)_4I$ crystal and the contributions from various degrees of freedom: (A) lattice vibration, (B) molecular libration, (C) known intramolecular vibration, (D) unknown intramolecular vibration, and (E) ($C_p - C_v$) correction.

heat capacities in series 7, where the sample was cooled to 354 K, about 20 K below the phase transition, agreed well with those in the other series, indicating that this phase transition does not show a remarkable thermal hysteresis in contrast to the previous DSC measurement.[32] We could not detect any thermal anomalies at 90 and 300 K, at which transitions concerning a change in the electronic structure have been reported.[24,25,28,29]

To evaluate the enthalpy and entropy acquisition due to the phase transition, we determined the normal heat capacity as follows. Normal heat capacity C_p (normal) may be approximated by the sum of contributions from lattice vibration (C_{lat}), molecular libration (C_{lib}), intramolecular vibration (C_{vib}), and the thermal dilation of the crystal (ΔC_{cor}):

$$C_p(\text{normal}) = C_{lat} + C_{lib} + \Delta C_{cor} \quad (1)$$

The heat capacity of the lattice vibration can be approximated by a Debye function, while the heat capacities of the molecular libration and the intramolecular vibration can be represented by Einstein functions. The last term in eq 1 corresponds to ($C_p - C_v$) correction and is approximated by the Nernst-Lindemann relation:

$$\Delta C_{cor} = C_p - C_v + AC_p^2T \quad (2)$$

The Einstein heat capacities for intramolecular vibrations were calculated for the known intramolecular vibrations assigned to $Pt_2(dta)_4I$ crystal ($22N_A$ degrees of freedom)[28] and dithioacetic acid ($32N_A$ degrees of freedom),[40] N_A being the Avogadro number. The Debye temperature of lattice vibration ($3N_A$ degrees of freedom), the Einstein temperature of molecular libration ($3N_A$ degrees of freedom), the four Einstein temperatures of unknown intramolecular vibrations ($33N_A$ degrees of freedom in total), and the correction coefficient A were estimated by fitting the heat capacity data below 270 K by nonlinear least-squares method. The derived parameters are tabulated in Table 2. The normal heat capacity curve thus obtained is shown together with the contribution of each term in Figure 2. Figure 2 indicates that the phase transition has not been completed yet.

The excess heat capacities calculated by subtracting the normal heat capacities from the experimental ones are displayed in Figure 3. The enthalpy and entropy of transition were estimated by integration of the obtained excess heat capacities with respect to T and ln T, respectively. The excess heat capacity above the highest measurement temperature was extrapolated by assuming the following equation:

$$\Delta C_p = a(T - b)^2 \quad (3)$$

where $a = 7.102 \times 10^{-2}$ J K^{-3} mol^{-1} and $b = 399.1$ K. The total enthalpy and entropy gains due to the transition thus estimated are $\Delta_{trs}H = (1.91 \pm 0.02)$ kJ mol^{-1} and $\Delta_{trs}S = (5.25 \pm 0.07)$ J K^{-1} mol^{-1}, respectively.

The phase transition at $T_{trs} = 373.4$ K seems to be of higher-order type rather than of first-order type because of no latent heat and no distinct thermal hysteresis. Shape of this phase transition also suggests a higher-order type. As described above, although the initial electrical conductivity measurements and single-crystal X-ray structure analyses[24,25] gave rise to an anomalous behavior of a large negative hysteresis in the phase

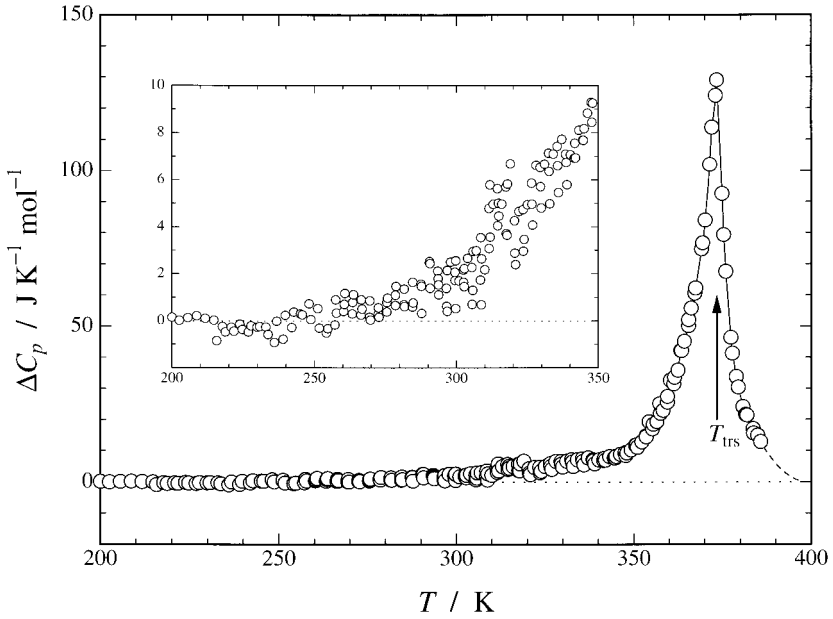

Figure 3. Excess heat capacities of $Pt_2(dta)_4I$ crystal. Dashed curve represents extrapolation of high-temperature tail of the phase transition by eq 3. Inset shows the excess heat capacities from 200 to 350 K.

transition temperature region between 300 and 350 K, the subsequent experiments[28,29] did not bring about such a behavior. The negative hysteresis in the initial experiments was probably caused by a considerably large lattice strain that would exist in the virginal crystal. Once the crystal experiences the phase transition, the lattice strain is removed and the crystal never gives rise to the 'negative' hysteresis. Such a behavior was also found in the present calorimetry. In series 1 where the virginal sample experienced the phase transition for the first time, the heat capacities were larger than those observed in the other series of measurements between 320 and 360 K below the transition temperature, and the sample exhibited an exothermic effect around this temperature range to release the lattice strain. No observation of such a negative hysteresis in this experiment would be attributed to a kind of annealing effect, because the measurement time is much longer for heat capacity experiment than for electrical conductivity and X-ray diffraction measurements.

The transition entropy for the phase transition at $T_{trs} = 373.4$ K, $\Delta_{trs}S = 5.25$ J K^{-1} mol^{-1}, is close to R ln 2 (= 5.76 J K^{-1} mol^{-1}), where R denotes the gas constant. This implies that this phase transition is of order−disorder type. The single-crystal X-ray crystallography[24,25,32] also revealed that the phase transition is of order−disorder type from being arranged in an ordered helical form of four dta ligand planes around the central Pt−Pt axis to dynamically jumping between two orientations. If the four dta ligands independently reorient between the two directions in the high-temperature phase, the transition entropy amounts to 4R ln 2 (= 23.1 J K^{-1} mol^{-1}). However, this is not the case. The fact that the experimental transition entropy is close to R ln 2 suggests that reorientation of the four dta ligands should be synchronized.

In the electrical conductivity measurement,[28,29] a tiny cusp was observed around 230 K, where the lattice constant a showed an anomalous negative temperature dependence.[31−33] Carefully inspecting the temperature dependence of the excess heat capacities in the inset of Figure 3, one can recognize that the excess heat capacity is increased above 230 K, forming the low-temperature tail of the phase transition occurring at 373.4 K. Therefore, it is very likely that the point at which the phase transition begins to become remarkable would correspond to the cusp appearing in the electrical conductivity and the negative temperature dependence of the lattice constant a.

The electrical conductivity, thermoelectric power, IR absorption, and magnetic susceptibility measurements[24−26,28−30] revealed that the metal−semiconductor transition occurs at T_{M-S} = 300 K, corresponding to a Mott transition from the one-dimensional metallic phase with mode (I) to the semiconducting phase with mode (III). On the other hand, the magnetic susceptibility and ^{129}I Mössbauer absorption measurements[27−29] suggested the existence of a spin-Peierls-like phase with mode (IV) below 90 K. However, the present calorimetric results indicate no thermal anomaly associated with the transitions at 90 and 300 K. We performed heat capacity measurement of a single crystal of $Pt_2(dta)_4I$ in the range from 22 to 317 K by ac calorimetry, which enables us to measure the heat capacity of a single crystal and to detect small thermal anomalies. However, no thermal anomaly was also detected around 90 and 300 K in this experiment. Generally the change of the crystal lattice involved in Mott transition is extremely small. Therefore the thermal anomaly due to the Mott transition at 300 K is, if any, too small to be detected by these calorimetries. On the other hand, since Peierls or spin-Peierls transition gives rise to a change of the crystal lattice due to dimerization, a thermal anomaly would be observed at 90 K if the transition actually occur. However, in the case of the $Pt_2(dta)_4I$ crystal, the spin in the crystal is still alive below 90 K, and hence, the lattice change would become very small. This might be the reason for no observation of a thermal anomaly at 90 K. It also seems to support this that the bridging I^- ions are situated at the midpoints of two $Pt_2(dta)_4$ dimers below and above the spin-Peierls-like transition temperature.[31]

TABLE 3: Standard Thermodynamic Functions of $Pt_2(dta)_4I$ Crystal (M = 881.78 g mol^{-1})

T/K	C_p° (J K^{-1} mol^{-1})	$(H_T^\circ - H_0^\circ)/T$ (J K^{-1} mol^{-1})	$S_T^\circ - S_0^\circ$ (J K^{-1} mol^{-1})	$-(G_T^\circ - H_0^\circ)/T$ (J K^{-1} mol^{-1})
5	1.874	0.4597	0.6092	0.1495
10	11.84	3.389	4.585	1.195
15	24.46	8.231	11.67	3.442
20	39.09	14.08	20.66	6.580
25	54.59	20.62	31.04	10.42
30	70.21	27.60	42.38	14.78
35	85.16	34.72	54.29	19.56
40	99.75	41.92	66.60	24.68
45	113.2	49.10	79.12	30.02
50	125.7	56.09	91.66	35.57
60	149.8	69.73	116.7	47.00
70	171.7	82.70	141.4	58.73
80	191.1	95.02	165.6	70.59
90	209.3	106.7	189.2	82.46
100	226.0	117.8	212.1	94.28
110	241.4	128.4	234.4	106.0
120	255.9	138.4	256.0	117.6
130	269.5	148.0	277.0	129.1
140	281.3	157.1	297.5	140.4
150	293.7	165.8	317.3	151.5
160	304.1	174.1	336.6	162.5
170	314.7	182.1	355.4	173.3
180	324.6	189.7	373.6	183.9
190	333.7	197.1	391.4	194.4
200	342.7	204.1	408.8	204.7
210	351.4	210.9	425.7	214.8
220	359.2	217.5	442.2	224.7
230	367.4	223.8	458.4	234.6
240	375.8	230.0	474.2	244.2
250	383.6	236.0	489.7	253.7
260	391.2	241.8	504.9	263.1
270	398.3	247.5	519.8	272.3
273.15	400.7	249.2	524.4	275.2
280	406.6	253.0	534.4	281.4
290	414.7	258.4	548.8	290.4
298.15	420.8	262.7	560.4	297.6
300	420.4	263.7	563.0	299.2
310	428.7	268.9	576.9	308.0
320	438.5	274.1	590.7	316.6
330	445.0	279.2	604.3	325.1
340	453.6	284.2	617.7	333.5
350	464.5	289.2	631.0	341.8
360	490.4	294.4	644.4	350.1
370	548.8	300.3	658.5	358.2
380	500.4	306.8	673.1	366.3

4. Conclusions

Heat capacity measurement of the halogen-bridged mixed-valence complex $Pt_2(dta)_4I$ has been carried out in the temperature region between 6 and 386 K by adiabatic calorimetry. The complex showed an order−disorder type of phase transition at T_{trs} = 373.4 K, from being arranged in an ordered helical form of four dta ligand planes around the central Pt−Pt axis to dynamically jumping between two orientations. Neither latent heat nor remarkable thermal hysteresis was observed for the phase transition. This suggests together with the shape of the phase transition that the phase transition is of higher-order rather than of first-order. The heat capacities of the virginal sample

were different from those of the sample which experienced the phase transition once. From this fact, the negative hysteresis observed in the initial experiments was probably caused by a considerably large lattice strain that would exist in the virginal crystal. The transition enthalpy and entropy were determined to be $\Delta_{trs}H = 1.91 \pm 0.02$ kJ mol^{-1} and $\Delta_{trs}S = 5.25 \pm 0.07$ J K^{-1} mol^{-1}, respectively. The transition entropy close to R ln 2 (= 5.76 J K^{-1} mol^{-1}) implies that the reorientational motion of the four dta ligands is synchronized. No thermal anomaly was detected around 300 and 90K, where a Mott transition from the one-dimensional metallic phase to the semiconducting phase and a spin-Peierls-like transition have been expected.

Acknowledgment. This study was partially supported by a Grant-in-Aid for Scientific Research on Priority Areas "Metal-Assembled Complexes" (Area No. 401/12023229) from the Ministry of Education, Science, Sports and Culture, Japan.

Appendix

Standard Thermodynamic Functions. Standard molar heat capacities, enthalpies, entropies, and Gibbs energies at rounded temperatures for the $Pt_2(dta)_4I$ crystal were calculated from the experimental heat capacity data and are summarized in Table 3. Extrapolation down to 0 K was carried out by using the following odd-order polynomial function

$$C_p/(\mathrm{J\,K^{-1}\,mol^{-1}}) = 1.357 \times 10^{-2}\,(T/\mathrm{K})^3 + 1.072 \times 10^{-4}\,(T/\mathrm{K})^5 - 2.255 \times 10^{-6}\,(T/\mathrm{K})^7 + 1.024 \times 10^{-8}\,(T/\mathrm{K})^9 \quad (4)$$

References and Notes

(1) Miller, J. S., Epstein, A. J., Eds. *Ann. N.Y. Acad. Sci.* **1978**, *313*, 1−828.
(2) Day, P. In *Low-Dimensional Cooperative Phenomena*; Keller, H. J., Ed.; Plenum: New York, 1974; p 191.
(3) Keller, H. J. In *Extended Linear Chain Compounds*; Miller, J. S., Ed.; Plenum: New York, 1982; Vol. 1, p 357.
(4) Clark, R. J. H. In *Mixed Valence Compounds*; Brown, D. E., Ed.; Reidel: Dordrecht, The Netherlands, 1982; p 271.
(5) Nasu, K. *J. Phys. Soc. Jpn.* **1983**, *52*, 3865.
(6) Nasu, K. *J. Phys. Soc. Jpn.* **1983**, *53*, 302.
(7) Toriumi, K.; Wada, Y.; Mitani, T.; Bandow, S.; Yamashita, M.; Fujii, Y. *J. Am. Chem. Soc.* **1989**, *111*, 2341.
(8) Chakraverty, B. K. *J. Phys. Fr. Lett.* **1979**, *40*, L99.
(9) Whangbo, M.; Foshee, M. *Inorg. Chem.* **1981**, *20*, 113.
(10) Gammel, G. T.; Saxena, A.; Batistic, I.; Bishop, A. R.; Phillpot, S. R. *Phys. Rev. B* **1992**, *45*, 6408.
(11) Che, C.-M.; Herbstein, F. H.; Schaefer, W. P.; Marsh, R. E.; Gray, H. B. *J. Am. Chem. Soc.* **1983**, *105*, 4604.
(12) Kurmoo, M.; Clark, R. J. H. *Inorg. Chem.* **1985**, *24*, 4420.
(13) Butler, L. G.; Zietlow, M. H.; Che, C.-M.; Schaefer, W. P.; Sridhar, S.; Grunthaner, P. J.; Swanson, B. I.; Clark, R. J. H.; Gray, H. B. *J. Am. Chem. Soc.* **1988**, *110*, 1155.
(14) Yamashita, M.; Toriumi K. *Inorg. Chim. Acta* **1990**, *178*, 143.
(15) Mitani, T.; Wada, Y.; Yamashita, M.; Toriumi, K.; Kobayashi, A.; Kobayashi, H. *Synth. Met.* **1994**, *64*, 291.
(16) Wada, Y.; Furuta, T.; Yamashita, M.; Toriumi, K. *Synth. Met.* **1995**, *70*, 1195.
(17) Yamashita, M.; Miya, S.; Kawashima, T.; Manabe, T.; Sonoyama, T.; Kitagawa, H.; Mitani, T.; Okamoto, H.; Ikeda, R. *J. Am. Chem. Soc.* **1999**, *121*, 2321.
(18) Kawashima, T.; Miya, S.; Manabe, T.; Yamashita, M.; Takizawa, K.; Ishii, T.; Tatsuzaka, H.; Sonoyama, T.; Kitagawa, H.; Mitani, T.; Matsuzaki, H.; Kishida, H.; Okamoto, H.; Ikeda, R. *Mol. Cryst. Liq. Cryst.* **2000**, *342*, 145.
(19) Bellito, C.; Flamini, A.; Gastaldi, L.; Scaramuzza, L. *Inorg. Chem.* **1983**, *22*, 444.
(20) Bellito, C.; Dessy, G.; Fares, U. *Inorg. Chem.* **1985**, *24*, 2815.
(21) Yamashita, M.; Wada, Y.; Toriumi, K.; Mitani, T. *Mol. Cryst. Liq. Cryst.* **1992**, *216*, 207.
(22) Shirotani, I.; Kawamura, A.; Yamashita, M.; Toriumi, K.; Kawamura, H.; Yagi, T. *Synth. Met.* **1994**, *64*, 265.
(23) Ikeda, R.; Kimura, N.; Ohki, H.; Furuta, T.; Yamashita, M. *Synth. Met.* **1995**, *71*, 1907.
(24) Kitagawa, H.; Onodera, N.; Ahn, J.-S.; Mitani, T.; Kim, M.; Ozawa, Y.; Toriumi, K.; Yasui, K.; Manabe, T.; Yamashita, M. *Mol. Cryst. Liq. Cryst.* **1996**, *285*, 311.
(25) Kitagawa, H.; Onodera, N.; Ahn, J.-S.; Mitani, T.; Toriumi, K.; Yamashita, M. *Synth. Met.* **1997**, *86*, 1931.
(26) Kitagawa, H.; Yamamoto, M.; Onodera, N.; Mitani, T. *Synth. Met.* **1999**, *103*, 2151.
(27) Kitagawa, H.; Sonoyama, T.; Mitani, T.; Seto, M.; Maeda, Y. *Synth. Met.* **1999**, *103*, 2159.
(28) Kitagawa, H.; Onodera, N.; Sonoyama, T.; Yamamoto, M.; Fukawa, T.; Mitani, T.; Seto, M.; Maeda, Y. *J. Am. Chem. Soc.* **1999**, *121*, 10068.
(29) Kitagawa, H.; Mitani, T. *Coord. Chem. Rev.* **1999**, *190−192*, 1169.
(30) Kitagawa, H.; Onodera, N.; Mitani, T. *Mol. Cryst. Liq. Cryst.* **2000**, *342*, 111.
(31) Kitagawa, H.; Onodera, N.; Mitani, T. *Synth. Met.* **2001**, *116*, 401.
(32) Kim, M.; Tanaka, K.; Ozawa, Y.; Toriumi, K. Manuscript in preparation.
(33) Nakagami, S.; Kitagawa, H.; Yamamoto, M.; Sonoyama, T.; Morii, K.; Mitani, T. Manuscript in preparation.
(34) Borsch, S. A.; Prassides, K.; Robert, V.; Solonenko, A. O. *J. Chem. Phys.* **1998**, *109*, 4562.
(35) Robert, V.; Petit, S.; Borsch, S. A. *Inorg. Chem.* **1999**, *38*, 1573.
(36) Yamamoto, S. *J. Phys. Soc. Jpn.* **2000**, *69*, 13.
(37) Yamamoto, S. *Phys. Rev. B* **2001**, *63*, 125124.
(38) Kume, Y.; Miyazaki, Y.; Matsuo, T.; Suga, H. *J. Phys. Chem. Solids* **1992**, *53*, 1297.
(39) Saito, K.; Yamamura, Y.; Sorai, M. *Netsu Sokutei (Calor. Therm. Anal.)* **1998**, *25*, 150.
(40) Mecke, R.; Spiesecke, H. *Chem. Ber.* **1956**, *89*, 1110.